Robust, Efficient, and Long-Time Accurate Schemes to Simulate Gas Storage in Geological Formation

Huangxin Chen[1,2], Yuxiang Chen[2], Jisheng Kou[3], Shuyu Sun[1], Dunhui Xiao[1], Xuejun Xu[1], Haitao Yu[4], Tao Zhang[5], and Xiaoying Zhuang[6]

[1] School of Mathematical Sciences, Tongji University, Shanghai 200092, China.
`chx@xmu.edu.cn`, `suns@tongji.edu.cn`, `xiaodunhui@tongji.edu.cn`, and `xuxj@tongji.edu.cn`
[2] School of Mathematical Sciences and Fujian Provincial Key Laboratory on Mathematical Modeling and High Performance Scientific Computing, Xiamen University, Fujian 361005, China
`chx@xmu.edu.cn` and `chenyuxiang@stu.xmu.edu.cn`
[3] Key Laboratory of Rock Mechanics and Geohazards of Zhejiang Province and School of Civil Engineering, Shaoxing University, Shaoxing, Zhejiang 312000, China
`koujisheng@163.com`
[4] State Key Laboratory of Disaster Reduction in Civil Engineering, Tongji University, Shanghai 200092„ China
`yuhaitao@tongji.edu.cn`
[5] The School of New Energy, China University of Petroleum (East China), Qingdao, Shaodong 266580, China
`tao.zhang@upc.edu.cn`
[6] Department of Geotechnical Engineering, College of Civil Engneering, Tongji University, Shanghai 200092, China
`xiaoyingzhuang@tongji.edu.cn`

Abstract. In this paper, we consider the numerical simulation of gas storage in geological formation in the context of hydrogen underground storage and carbon dioxide geological sequestration. We constructs two energy-stable numerical schemes: one based on the energy factorization approach, which rigorously preserves the energy dissipation principle and combines discontinuous Galerkin approximations with mixed finite elements for spatial discretization; the other based on a stabilization approach, which conserves the original energy functional, has an adaptive stabilization parameter and time-stepping strategy, and ensures the boundedness of molar density. Through numerical experiments with methane gas, our schemes are validated in terms of capturing coupled hydro-mechanical processes, handling strong nonlinearities, and maintaining conservation properties.

Keywords: Efficiency of numerical schemes · Gas storage in geological Formation · Temporal discretization · Long-time accurate simulation · Spatial discretization · Robustness.

ICCS Camera Ready Version 2025
To cite this paper please use the final published version:
DOI: `10.1007/978-3-031-97632-2_15`

1 Introduction

Geological sequestration of carbon dioxide and underground storage of hydrogen are two critical applications of geological storage technologies, with profound implications for global energy utilization and environmental protection [5, 10]. Numerical simulation plays a pivotal role in geological storage research, but its accuracy and stability are influenced by various factors. For instance, higher-order numerical algorithms are required to improve computational precision while ensuring local mass conservation and avoiding numerical dispersion and non-physical oscillations. Additionally, large time-step calculations must balance computational efficiency with stability and reliability. Furthermore, when simulating multiphase flow in geological environments, the phase behavior of fluids is particularly critical, especially the impact of temperature, pressure, and salt concentration on interfacial tension, which further complicates the simulation [15, 17].

This study focuses on the numerical simulation of single-phase gas flow with compressible gas and rock in the context of hydrogen underground storage and carbon dioxide geological sequestration, exploring the construction of governing equations, numerical challenges, and corresponding strategies. The numerical implementation of our physical model must strictly adhere to thermodynamic consistency, as methods violating this principle can lead to unphysical or unstable simulation results [5, 11]. Various approaches have been developed to handle Helmholtz free energy in numerical schemes. The convex splitting method [9] has been widely used for both single- and multi-component systems, providing nonlinear energy-stable schemes. However, it requires solving nonlinear equations, often at high computational cost. Alternative strategies include stabilization methods [19], exponential time-differencing [7], and the Invariant Energy Quadratization (IEQ) [21] and Scalar Auxiliary Variable (SAV) approaches [18]. While the IEQ and SAV methods yield linear, easily implementable energy-stable schemes, their modified energy functionals deviate from the original. The Energy Factorization (EF) method [12, 13] provides an alternative approach that maintains the original energy dissipation structure while offering computational efficiency. The stabilization method proposed by [14] integrates features from existing approaches, preserving the original energy functional and enabling linear energy-stable formulations. Maintaining the physical bounds of molar density $0 < c < \frac{1}{\beta}$ is critical in simulating compressible gas flow through porous media. Deviations from these bounds yield non-physical solutions, necessitating numerical schemes that intrinsically enforce these constraints. Recent advances in bounding techniques include the constraint enforcement methods such as Lagrange multiplier approaches [2] and variational formulations [8], a posteriori corrections such as post-processing [22] and cut-off strategies [20], and the energy-based methods such as nonlinear convex splitting [1, 6].

The paper is organized as follows. In section 2, we introduce the formulation of gas flow model with rock compressibility. In section 3, we introduce two energy-stable numerical schemes and discuss the properties they satisfy. In section 4, numerical results are presented to verify the features of the proposed scheme.

ICCS Camera Ready Version 2025
To cite this paper please use the final published version:
DOI: 10.1007/978-3-031-97632-2_15

2 Mathematical Model of Gas Flow In Poroelastic Media

For the convenience of presentation, we focus on single-phase gas flow with compressible gas and rock. We consider a fully coupled thermodynamic mathematical model for single-phase gas flow in porous media, incorporating the compressibility of both gas and rock.

$$\nabla \cdot \sigma(\boldsymbol{u}_s, p) = 0, \qquad \text{in } \Omega_t =: \Omega \times (0,t), \tag{1a}$$

$$\frac{\partial(\phi c)}{\partial t} + \nabla \cdot (\boldsymbol{u}_f c) = 0, \qquad \text{in } \Omega_t, \tag{1b}$$

$$\boldsymbol{u}_f = -\lambda(\phi) c \nabla \mu, \qquad \text{in } \Omega_t, \tag{1c}$$

$$p = c\mu(c) - f(c), \qquad \text{in } \Omega_t, \tag{1d}$$

$$\frac{\partial \phi}{\partial t} = \frac{1}{N}\frac{\partial p}{\partial t} + \alpha \nabla \cdot \mathbf{v}_s, \qquad \text{in } \Omega_t, \tag{1e}$$

where $\lambda(\phi) = \frac{\kappa(\phi)}{\nu}$ is the mobility, ν is the viscosity of gas, $\kappa(\phi) = \kappa_0(\frac{\phi}{\phi_r})^3(\frac{1-\phi_r}{\phi})^2$ is the permeability, κ_0 is the initial intrinsic permeability and ϕ_r is the porosity at the reference pressure. $\sigma(\boldsymbol{u}_s, p) = 2\eta\varepsilon(\boldsymbol{u}_s) + \gamma \operatorname{div}(\boldsymbol{u}_s)\mathbf{I} - \alpha p \mathbf{I}$ is the stress tensor, $\varepsilon(\boldsymbol{u}_s) = \frac{1}{2}(\nabla \boldsymbol{u}_s + \nabla \boldsymbol{u}_s^T)$ is the strain tensor, $\mathbf{I}$ is the unit tensor, $\boldsymbol{u}_s$ is the displacement of solid, $\mathbf{v}_s = \frac{\partial \boldsymbol{u}_s}{\partial t}$ is the velocity of solid, η and γ are the Lamé parameters, α is the Biots coefficient, N is the Biot's modulus, c is the molar density of gas. The Helmholtz free energy density $f(c)$ and chemical potential μ determined by the Peng-Robinson equation of state have the following expression

$$f(c) = f_{ide}(c) + f_{rep}(c) + f_{att}(c), \tag{2a}$$

$$f_{\text{ide}}\,(c) = cRT\ln(c),\ f_{\text{rep}}\,(c) = -cRT\ln(1-\beta c), \tag{2b}$$

$$f_{att}(c) = \frac{b(T)c}{2\sqrt{2}\beta} \ln\left(\frac{1+(1-\sqrt{2})\beta c}{1+(1+\sqrt{2})\beta c}\right), \tag{2c}$$

$$\mu(c) = f'(c). \tag{2d}$$

The pressure is given by the volumetric EoS: $p = \frac{cRT}{1-\beta c} - \frac{bc^2}{1+2\beta c - \beta^2 c^2}$. In order to close the system, the following boundary conditions are imposed

$$\sigma(\boldsymbol{u}_s, p) \cdot \boldsymbol{n} = 0, \qquad \text{on } \partial\Omega, \tag{3}$$

$$\boldsymbol{u}_f \cdot \boldsymbol{n} = 0, \qquad \text{on } \partial\Omega. \tag{4}$$

The total free energy of (1) and (3) in Ω can be defined as

$$E(t) = \int_\Omega \left(\phi f(c) + \frac{1}{2}\sigma_e(\boldsymbol{u}_s) : \varepsilon(\boldsymbol{u}_s) + \frac{1}{2N}p^2\right)\, d\boldsymbol{x}. \tag{5}$$

3 Two Energy-Stable Numerical Schemes

For thermodynamically consistent models of gas flow in porous media, it is essential to construct numerical schemes that strictly adhere to the energy dissipation

ICCS Camera Ready Version 2025
To cite this paper please use the final published version:
DOI: 10.1007/978-3-031-97632-2_15

law, thereby improving computational stability and efficiency. This section introduces two energy-stable numerical schemes based on an improved energy factorization method and a stabilization strategy, respectively, to guarantee energy stability in numerical computations and optimize computational efficiency.

3.1 Energy-Stable Scheme Based on Energy Factorization Approach

The first numerical approach utilizes an energy factorization method for treating the Helmholtz free energy density while implementing a semi-implicit time-stepping formulation. This method rigorously preserves the energy dissipation principle by precisely computing the pressure field through chemical potential and Helmholtz free energy. The spatial discretization framework combines discontinuous Galerkin approximations [16] with mixed finite elements, incorporating upwind flux treatment to maintain both mass conservation properties and numerical stability.

The time semi-discretized chemical potential μ^{n+1} is derived through a thermodynamically consistent energy factorization methodology [13], framework for constructing energy-stable semi-discrete chemical potentials by leveraging the convexity and concavity properties of different components of the free energy function. we get the linearized semi-discretized chemical potential

$$\mu^{n+1} = \mu_{ir}\left(c^{n+1}, c^{n}\right) + \mu_{att}\left(c^{n+1}, c^{n}\right)$$

where

$$\mu_{ir}\left(c^{n+1}, c^{n}\right) = RT\left(\ln\left(c^{n}\right) - \ln\left(1-\beta c^{n}\right)\right) + RTc^{n+1}\left(\frac{1}{c^{n}} + \frac{\beta}{1-\beta c^{n}}\right), \tag{6a}$$

$$\begin{aligned}\mu_{att}\left(c^{n+1}, c^{n}\right) =& \frac{b}{2\sqrt{2}\beta}\left(\ln\left(1+(1-\sqrt{2})\beta c^{n}\right) + \frac{(1-\sqrt{2})\beta c^{n+1}}{1+(1-\sqrt{2})\beta c^{n}}\right) \\ & - \frac{b}{2\sqrt{2}\beta}\left(\ln\left(1+(1+\sqrt{2})\beta c^{n}\right) + \frac{(1+\sqrt{2})\beta c^{n}}{1+(1+\sqrt{2})\beta c^{n}}\right).\end{aligned} \tag{6b}$$

Building upon the semi-discrete formulation of the chemical potential derived above, we rigorously establish the following free energy dissipation inequality that governs the thermodynamic consistency of the numerical scheme:

$$\begin{aligned}& f_{ide}\left(c^{n+1}\right) + f_{rep}\left(c^{n+1}\right) - f_{ide}\left(c^{n}\right) - f_{rep}\left(c^{n}\right) \\ \leq\; & \mu_{\mathrm{ir}}\left(c^{n+1}, c^{n}\right)\left(c^{n+1} - c^{n}\right),\end{aligned} \tag{7}$$

$$f_{att}\left(c^{n+1}\right) - f_{att}\left(c^{n}\right) \leq \mu_{att}\left(c^{n+1}, c^{n}\right)\left(c^{n+1} - c^{n}\right). \tag{8}$$

By systematically integrating the discrete chemical potential formulation derived through energy factorization method [13] with a semi-implicit Euler temporal

ICCS Camera Ready Version 2025
To cite this paper please use the final published version:
DOI: 10.1007/978-3-031-97632-2_15

discretization framework, we rigorously construct the following energy-stable semi-discrete system:

$$-\nabla\cdot\sigma(\boldsymbol{u}_s^{n+1},p^{n+1})=0, \tag{9a}$$

$$D_\tau(\phi^{n+1}c^{n+1})+\nabla\cdot(\boldsymbol{u}_f^{n+1}c^n)=0, \tag{9b}$$

$$\boldsymbol{u}_f^{n+1}=-\lambda(\phi^n)c^n\nabla\mu^{n+1}, \tag{9c}$$

$$p^{n+1}=c^n\mu^{n+1}-f(c^n), \tag{9d}$$

$$D_\tau\phi^{n+1}=\frac{1}{N}D_\tau p^{n+1}+\alpha\nabla\cdot D_\tau\boldsymbol{u}_s^{n+1}. \tag{9e}$$

We employ a temporally uniform discretization parameter defined as $\tau=t_{n+1}-t_n$, where B^n represents the discrete approximation of molar density at temporal node t_n The backward difference operator is systematically defined for all primary variables $B\in\{\boldsymbol{u}_s,\phi,p,c,E\}$ through the discrete temporal derivative:

$$D_\tau B^{n+1}:=\frac{B^{n+1}-B^n}{\tau}.$$

The energy dissipation property of system (9a), rigorously proven in Theorem 3.2 of [4].

Theorem 1. *([4]) Let $\sigma(\boldsymbol{u}_s^{n+1},p^{n+1})\cdot\boldsymbol{n}=0,\boldsymbol{u}_f^{n+1}\cdot\boldsymbol{n}=0$ on the boundary $\partial\Omega$, where $\boldsymbol{n}$ denotes the normal unit outward vector to $\partial\Omega$. We assume that $0<c^n<\frac{\varrho}{\beta},n\geq 0$. Then the scheme (9) follows an energy dissipation law as*

$$D_\tau E^{n+1}\leq 0,$$

where

$$E^{n+1}=\int_\Omega\left(\phi^{n+1}f(c^{n+1})+\frac{1}{2}\sigma_e(\boldsymbol{u}_s^{n+1}):\varepsilon(\boldsymbol{u}_s^{n+1})+\frac{1}{2N}|p^{n+1}|^2\right)\,d\boldsymbol{x}$$

is the semidiscrete total energy at the time t_{n+1}.

Let $\mathcal{K}_h$ be a family of nondegenerate, quasi-uniform partitions of Ω composed of triangles or quadrilaterals if $d=2$, or tetrahedra, prisms, or hexahedra if $d=3$. Define $\mathcal{E}_h$ as the set of all faces ($d=3$) or edges ($d=2$) of $\mathcal{K}_h$, and let h_T be the diameter of any element $K\in\mathcal{K}_h$. The set of interior edges or faces in $\mathcal{E}_h$ is denoted by $\mathcal{E}_h^I$. The standard finite element space of d-dimensional vector fields, whose components are piecewise linear polynomials, is given by:

$$\mathcal{V}_h:=\left\{\psi\in[L^2(\Omega)]^d:\psi|_K\in\mathbb{P}_1^d(K),\forall K\in\mathcal{K}_h\right\}.$$

We now define the average and jump operators for $\psi\in\mathcal{V}$. Given two neighboring elements $K_i,K_j\in\mathcal{K}_h$ and an interface $e=\partial K_i\cap\partial K_j\in\mathcal{E}_h^I$ with outward unit normal vector $\boldsymbol{n}_e$ exterior to K_i, we define:

$$\{\psi\}:=\frac{1}{2}((\psi|_{K_i})|_e+(\psi|_{K_j})|_e),\quad [\psi]:=\left(\psi|_{K_i}\right)\big|_e-\left(\psi|_{K_j}\right)|_e,$$

ICCS Camera Ready Version 2025
To cite this paper please use the final published version:
DOI: 10.1007/978-3-031-97632-2_15

here, $\psi|_{K_i}$ represents the value of ψ in K_i.

The inner product on an edge or face e is given by $\langle \cdot, \cdot \rangle_e$, the associated norms are denoted by $\| \cdot \|_{L^2(e)}$. Next, we introduce the lowest-order Raviart-Thomas (RT_0) mixed finite element space, which will be used in the spatial discretization. On a simplicial mesh, the space RT_0 is defined as: $RT_0 = [\mathbb{P}_0]^d + \boldsymbol{x}\mathbb{P}_0$, where $\mathbb{P}_0$ represents the space of piecewise constant functions. We define the following finite element spaces:

$$\begin{aligned}
\mathcal{U}_h &= \{\mathbf{v} \in H(\mathrm{div}, \Omega) : \mathbf{v}|_K \in RT_0(K), \forall K \in \mathcal{K}_h\}, \\
\mathcal{Q}_h &= \left\{q \in L^2(\Omega) : q|_K \in \mathbb{P}_0(K), \forall K \in \mathcal{K}_h\right\},
\end{aligned}$$

where $H(\mathrm{div}, \Omega)$ is defined as: $H(\mathrm{div}, \Omega) = \left\{\mathbf{v} \in [L^2(\Omega)]^d : \nabla \cdot \mathbf{v} \in L^2(\Omega)\right\}$.

Additionally, we define the space with homogeneous normal boundary conditions:

$$\mathcal{U}_h^0 = \{\mathbf{v} \in \mathcal{U}_h : \mathbf{v} \cdot \boldsymbol{n} = 0 \text{ on } \partial\Omega\}.$$

Next, we develop a fully discrete numerical scheme using the mixed finite element method with upwind scheme that strictly maintains both energy stability and mass conservation. The scheme combines an upwind treatment of advection terms with a carefully balanced implicit-explicit temporal discretization, ensuring robust performance.

For any $\mathbf{v}_h \in \mathcal{V}_h$, $\mathbf{w}_h \in \mathcal{U}_h^0$, $q_h, z_h, \varphi_h \in \mathcal{Q}_h$, we determine $\boldsymbol{u}_{s,h}^{n+1} \in \mathcal{V}_h$, $\boldsymbol{u}_{f,h}^{n+1} \in \mathcal{U}_h$, $c_h^{n+1}, \phi_h^{n+1}, p_h^{n+1} \in \mathcal{Q}_h$ such that:

$$\mathcal{A}(\boldsymbol{u}_{s,h}^{n+1}, p_h^{n+1}, \mathbf{v}_h) = 0, \tag{10a}$$

$$(D_\tau(\phi_h^{n+1} c_h^{n+1}), q_h) + \sum_{e \in \mathcal{E}_h^I} \langle c_h^{n*} \boldsymbol{u}_{f,h}^{n+1} \cdot \boldsymbol{n}, [q_h] \rangle_e = 0, \tag{10b}$$

$$(\lambda^{-1}(\phi_h^n) \boldsymbol{u}_{f,h}^{n+1}, \mathbf{w}_h) = \sum_{e \in \mathcal{E}_h^I} \langle [\mu_h^{n+1}], c_h^{n*} \mathbf{w}_h \cdot \boldsymbol{n} \rangle_e, \tag{10c}$$

$$(p_h^{n+1}, z_h) = (c_h^n \mu_h^{n+1} - f(c_h^n), z_h), \tag{10d}$$

$$\begin{aligned}
(D_\tau \phi_h^{n+1}, \varphi_h) = {} & \frac{1}{N}(D_\tau p_h^{n+1}, \varphi_h) + \alpha(D_\tau(\nabla \cdot \boldsymbol{u}_{s,h}^{n+1}), \varphi_h) \\
& - \alpha \sum_{e \in \mathcal{E}_h^I} \langle \{\varphi_h \boldsymbol{n}_e\}, [D_\tau \boldsymbol{u}_{s,h}^{n+1}] \rangle_e.
\end{aligned} \tag{10e}$$

The bilinear form $\mathcal{A}$ is defined as:

$$\begin{aligned}
\mathcal{A}(\boldsymbol{u}_{s,h}, p_h, \mathbf{v}_h) := {} & \sum_{K \in \mathcal{K}_h} (\sigma_e(\boldsymbol{u}_{s,h}), \varepsilon(\mathbf{v}_h))_K - \sum_{e \in \mathcal{E}_h^I} \langle \{\sigma_e(\boldsymbol{u}_{s,h}) \boldsymbol{n}_e\}, [\mathbf{v}_h] \rangle_e \\
& - \alpha \sum_{K \in \mathcal{K}_h} (p_h, \nabla \cdot \mathbf{v})_K + \alpha \sum_{e \in \mathcal{E}_h^I} \langle \{p_h \boldsymbol{n}_e\}, [\mathbf{v}_h] \rangle_e \\
& - \sum_{e \in \mathcal{E}_h^I} \langle [\boldsymbol{u}_{s,h}], \{\sigma_e(\mathbf{v}_h) \boldsymbol{n}_e\} \rangle_e + \sum_{e \in \mathcal{E}_h^I} \frac{\varsigma 2}{h_e} \langle [\boldsymbol{u}_{s,h}], [\mathbf{v}_h] \rangle_e.
\end{aligned} \tag{11}$$

Here, ς_2 is a penalty parameter and $h_e = |e|^{\frac{1}{d-1}}$.

To handle rock compressibility, the scheme (10) forms a nonlinear system, which we solve iteratively. Given c_h^n, $\boldsymbol{u}_{s,h}^n$, $\boldsymbol{u}_{f,h}^n$, ϕ_h^n, and p_h^n, we initialize:

$$\begin{aligned} &c_h^{n+1,0} = c_h^n, \quad \boldsymbol{u}_{s,h}^{n+1,0} = \boldsymbol{u}_{s,h}^n, \quad \boldsymbol{u}_{f,h}^{n+1,0} = \boldsymbol{u}_{f,h}^n, \\ &\phi_h^{n+1,0} = \phi_h^n, \quad p_h^{n+1,0} = p_h^n. \end{aligned}$$

For $l \geq 0$, we solve the linear system:

$$\begin{aligned} &\mathcal{A}(\boldsymbol{u}_{s,h}^{n+1,l+1}, p_h^{n+1,l+1}, \mathbf{v}_h) = 0, \\ &(D\tau(\phi_h^{n+1,l} c_h^{n+1,l+1}), q_h) + \sum_{e \in \mathcal{E}_h^I} \langle c_h^{n*} \boldsymbol{u}_{f,h}^{n+1,l+1} \cdot \boldsymbol{n}, [q_h] \rangle_e = 0, \\ &(\lambda^{-1}(\phi_h^n) \boldsymbol{u}_{f,h}^{n+1,l+1}, \mathbf{w}_h) = \sum_{e \in \mathcal{E}_h^I} \langle [\mu_h^{n+1,l+1}], c_h^{n*} \mathbf{w}_h \cdot \boldsymbol{n} \rangle_e, \\ &(p_h^{n+1,l+1}, z_h) = (c_h^n \mu_h^{n+1,l+1} - f(c_h^n), z_h), \\ &(D_\tau \phi_h^{n+1,l+1}, \varphi_h) = \frac{1}{N}(D_\tau p_h^{n+1,l+1}, \varphi_h) + \alpha(D_\tau(\nabla \cdot \boldsymbol{u}_{s,h}^{n+1,l+1}), \varphi_h) \\ &- \alpha \sum_{e \in \mathcal{E}_h^I} \langle \{\varphi_h \boldsymbol{n}_e\}, [D_\tau \boldsymbol{u}_{s,h}^{n+1,l+1}] \rangle_e. \end{aligned}$$

Theorem 2. *([4]) Let* $\sigma(\boldsymbol{u}_{s,h}^{n+1}, p_h^{n+1}) \cdot \boldsymbol{n} = 0, \boldsymbol{u}_{f,h}^{n+1} \cdot \boldsymbol{n} = 0$ *on the boundary* $\partial\Omega$*, where* $\boldsymbol{n}$ *denotes the normal unit outward vector to* $\partial\Omega$*. We assume that* $0 < c_h^n < \frac{\varrho}{\beta}, n \geq 0$*. Then the scheme* (10) *follows an energy dissipation law as*

$$D_\tau E_h^{n+1} \leq - \sum_{K \in \mathcal{K}_h} \int_K \lambda^{-1}(\phi_h^n) |\boldsymbol{u}_{f,h}^{n+1}|^2 \, d\boldsymbol{x} \leq 0.$$

3.2 Stabilization-Based Energy-Stable Scheme Approach

The second numerical formulation implements a stabilization methodology that rigorously conserves the original energy functional while establishing provably stable linear discretizations. During each temporal iteration, the stabilization parameter undergoes adaptive modification through an explicit closed-form relation, ensuring strict adherence to fundamental energy dissipation principles. To optimize computational performance, the algorithm incorporates an adaptive temporal discretization framework that strategically allocates computational resources while maintaining solution accuracy and boundedness. The time step size explicitly derived from local solution characteristics at each linear iteration. Spatial discretization is achieved through a mixed finite element formulation with consistent upwind flux approximation, ensuring discrete stability while exactly preserving mass conservation properties.

The discrete chemical potential incorporates a dynamically adjusted stabilization term $\mu^{n+1} = \mu(c^n) + \theta_n RT \underbrace{\frac{c^{n+1} - c^n}{c^n(1-\beta c^n)^2}}_{\zeta^{n+1}}$, where ζ^{n+1} represents the stabilization term, θ_n is the stabilization parameter. By the Taylor expansion and assuming that ξ is a number between c^n and c^{n+1}, we have $f\left(c^{n+1}\right) - f\left(c^n\right) = \mu\left(c^n\right)\left(c^{n+1} - c^n\right) + \frac{f''(\xi)}{2}\left(c^{n+1} - c^n\right)^2$. In view of the above stabilized chemical potential, we further obtain

$$\begin{aligned} f\left(c^{n+1}\right) - f\left(c^n\right) = {} & \mu^{n+1}\left(c^{n+1} - c^n\right) \\ & + \left(\frac{f''(\xi)}{2} - \frac{\theta_n RT}{c^n\left(1 - \beta c^n\right)^2}\right)\left(c^{n+1} - c^n\right)^2 . \end{aligned} \tag{12}$$

By choosing a suitable stabilization parameter θ_n, we can obtain the following inequality.

$$f\left(c^{n+1}\right) - f\left(c^n\right) \le \mu^{n+1}\left(c^{n+1} - c^n\right), \tag{13}$$

then, we can get

$$\begin{aligned} \phi^{n+1} f\left(c^{n+1}\right) - \phi^n f\left(c^n\right) = {} & f\left(c^n\right)\left(\phi^{n+1} - \phi^n\right) \\ & + \phi^{n+1}\left(f\left(c^{n+1}\right) - f\left(c^n\right)\right) \\ \le {} & f\left(c^n\right)\left(\phi^{n+1} - \phi^n\right) + \phi^{n+1}\mu^{n+1}\left(c^{n+1} - c^n\right), \end{aligned} \tag{14}$$

the specific choice of the stabilization term θ_n can be found in paper [3].

Building upon the semi-discrete stabilization framework for the chemical potential, we now present the complete space-time discrete formulation. This scheme systematically integrates the stabilization strategy with a mixed finite element discretization in space and an implicit-explicit temporal scheme, ensuring both thermodynamic consistency and numerical robustness: For any $\mathbf{v}_h \in \mathcal{V}_h, \mathbf{w}_h \in \mathcal{U}_h^0, q_h, z_h, \varphi_h \in \mathcal{Q}_h$, we find $\boldsymbol{u}_{s,h}^{n+1} \in \mathcal{V}_h, \boldsymbol{u}_{f,h}^{n+1} \in \mathcal{U}_h, c_h^{n+1}, \phi_h^{n+1}, p_h^{n+1} \in \mathcal{Q}_h$ such that

$$\mathcal{A}(\boldsymbol{u}_{s,h}^{n+1}, p_h^{n+1}, \mathbf{v}_h) = 0, \tag{15a}$$

$$\begin{aligned} (D_\tau(\phi_h^{n+1} c_h^{n+1}), q_h) + & \sum_{e \in \mathcal{E}_h^I} \langle c_h^{n*} \boldsymbol{u}_{f,h}^{n+1} \cdot \boldsymbol{n}, [q_h] \rangle_e \\ & + \sum_{e \in \mathcal{E}_h^I} \frac{\varsigma_1}{h_e} \langle [\mu_h^{n+1}], [q_h] \rangle = 0, \end{aligned} \tag{15b}$$

$$(\lambda^{-1}(\phi_h^n) \boldsymbol{u}_{f,h}^{n+1}, \mathbf{w}_h) = \sum_{e \in \mathcal{E}_h^I} \langle [\mu_h^{n+1}], c_h^{n*} \mathbf{w}_h \cdot \boldsymbol{n} \rangle_e, \tag{15c}$$

$$(p_h^{n+1}, z_h) = (c_h^n \mu_h^{n+1} - f(c_h^n), z_h), \tag{15d}$$

$$\begin{aligned} (D_\tau \phi_h^{n+1}, \varphi_h) = {} & \frac{1}{N}(D_\tau p_h^{n+1}, \varphi_h) + \alpha(D_\tau(\nabla \cdot \boldsymbol{u}_{s,h}^{n+1}), \varphi_h) \\ & - \alpha \sum_{e \in \mathcal{E}_h^I} \langle \{\varphi_h \boldsymbol{n}_e\}, [D_\tau \boldsymbol{u}_{s,h}^{n+1}] \rangle_e, \end{aligned} \tag{15e}$$

ICCS Camera Ready Version 2025
To cite this paper please use the final published version:
DOI: 10.1007/978-3-031-97632-2_15

Since the equation (15b) is nonlinear, we use the linear iteration method to solve the equations (15).

$$\mathcal{A}(\mathbf{u}_{s,h}^{n+1,l+1}, p_h^{n+1,l+1}, \mathbf{v}_h) = 0, \tag{16}$$

$$\begin{aligned}(\frac{\phi_h^{n+1,l} c_h^{n+1,l+1} - \phi_h^n c_h^n}{\tau}, q_h) + \sum_{e \in \mathcal{E}_h^I} \langle c_h^{n*} \mathbf{u}_{f,h}^{n+1,l} \cdot \boldsymbol{n}, [q_h] \rangle_e \\ + \sum_{e \in \mathcal{E}_h^I} \frac{\varsigma_1}{h_e} \langle [\mu_h^{n+1,l+1}], [q_h] \rangle_e = 0,\end{aligned} \tag{17}$$

$$(\lambda^{-1}(\phi_h^n) \mathbf{u}_{f,h}^{n+1,l+1}, \mathbf{w}_h) = \sum_{e \in \mathcal{E}_h^I} \langle [\mu_h^{n+1,l+1}], c_h^{n*} \mathbf{w}_h \cdot \boldsymbol{n} \rangle_e, \tag{18}$$

$$(p_h^{n+1,l+1}, z_h) = (c_h^n \mu_h^{n+1,l+1} - f(c_h^n), z_h), \tag{19}$$

$$\begin{aligned}(D_\tau \phi_h^{n+1,l+1}, \varphi_h) = \frac{1}{N}(D_\tau p_h^{n+1,l+1}, \varphi_h) + \alpha (D_\tau (\nabla \cdot \mathbf{u}_{s,h}^{n+1,l+1}), \varphi_h) \\ - \alpha \sum_{e \in \mathcal{E}_h^I} \langle \{\varphi_h \boldsymbol{n}_e\}, [D_\tau \mathbf{u}_{s,h}^{n+1,l+1}] \rangle_e.\end{aligned} \tag{20}$$

As rigorously proven in reference [3], the fully discrete scheme adopted in this paper achieves dynamic adaptive time step adjustment while ensuring the boundedness of the molar density.

Theorem 3. *([3]) Assume that* $0 < \varrho_0 \leq \beta c_h^n \leq \varrho < 1$ *and the boundary condition* (3) *holds. For* $n \geq 0$ *and given constants* $0 < \delta_1 < 1$ *and* $0 < \delta_2 < 1$*, if the time step size* τ_n^l *satisfies*

$$\tau_n^l = \min_{K \in \mathcal{K}_h} \left(\frac{\left(\phi_h^{n+1,l} c_h^n \left(1 - \beta c_h^n\right)^2 \delta_1 - (\phi_h^{n+1,l} - \phi_h^n) c_h^n\right) |K|}{\sum\limits_{e \in \partial K_{\boldsymbol{u}_{f,h}}^+} c_h^n \boldsymbol{u}_{f,h}^{n+1,l} \cdot \boldsymbol{n} |e| + \sum\limits_{e \in \partial K_\mu^+} \frac{\varsigma_1}{h_e} [\mu(c_h^n)] |e| + \epsilon}, \right. \tag{21}$$

$$\left. \frac{\left(\phi_h^{n+1,l} c_h^n \left(1 - \beta c_h^n\right)^2 \delta_2 + (\phi_h^{n+1,l} - \phi_h^n) c_h^n\right) |K|}{-\left(\sum\limits_{e \in \partial K_{\boldsymbol{u}_{f,h}}^-} c_h^{n*} \boldsymbol{u}_{f,h}^{n+1,l} \cdot \boldsymbol{n} |e| + \sum\limits_{e \in \partial K_\mu^-} \frac{\varsigma_1}{h_e} [\mu(c_h^n)] |e| \right) + \epsilon}, \tau_{max} \right),$$

where $\epsilon > 0$ *is a very small constant to avoid zero denominator,* τ_{max} *is the allowed maximum time step size to guarantee the accuracy of numerical solutions and* $\partial K_{\boldsymbol{u}_{f,h}}^+ = \{e \in \partial K : \boldsymbol{u}_{f,h}^{n+1} \cdot \boldsymbol{n}|_e > 0, \forall K \in \mathcal{K}_h\}$, $\partial K_{\boldsymbol{u}_{f,h}}^- = \{e \in \partial K : \boldsymbol{u}_{f,h}^{n+1} \cdot \boldsymbol{n}|_e < 0, \forall K \in \mathcal{K}_h\}$, $\partial K_\mu^- = \{e \in \partial K : [\mu(c_h^n)] < 0, \forall K \in \mathcal{K}_h\}, \partial K_\mu^+ = \{e \in \partial K : [\mu(c_h^n)] > 0, \forall K \in \mathcal{K}_h\}$*. Then* $c_h^{n+1,l+1}$ *satisfies*

$$0 < (1 - \delta_1 \left(1 - \beta c_h^n\right)^2) c_h^n \leq c_h^{n+1,l+1} \leq (1 + \delta_2 \left(1 - \beta c_h^n\right)^2) c_h^n < \frac{1}{\beta}.$$

It is also proved in paper [3] that the fully discrete numerical format based on the stabilization method satisfies the properties of energy dissipation.

ICCS Camera Ready Version 2025
To cite this paper please use the final published version:
DOI: 10.1007/978-3-031-97632-2_15

Theorem 4. *([3]) Assume that the boundary condition* (3) *holds,* $0 < \epsilon \leq c_h^n \leq \frac{\varrho}{\beta} < \frac{1}{\beta}$. *The stabilization parameter* θ_n *is taken as follows:*

$$\theta_n = \max_{K \in \mathcal{K}_h} \left\{ 1, \frac{\left(1 - \beta c_h^n\right)^2}{\chi_1^n \left(1 - \chi_1^n \beta c_h^n\right)^2}, \frac{\left(1 - \beta c_h^n\right)^2}{\chi_2^n \left(1 - \chi_2^n \beta c_h^n\right)^2} \right\}, \tag{22}$$

where $\chi_1^n = 1 - \delta_1 \left(1 - \beta c_h^n\right)^2$, $\chi_2^n = 1 + \delta_2 \left(1 - \beta c_h^n\right)^2$. *The total free energy generated by the scheme* (10) *is dissipated as*

$$D_\tau E_h^{n+1} \leq 0,$$

where

$$\begin{aligned} E_h^{n+1} = &\sum_{K \in \mathcal{K}_h} \int_K \left(\phi_h^{n+1} f(c_h^{n+1}) + \frac{1}{2} \sigma_e(\boldsymbol{u}_{s,h}^{n+1}) : \varepsilon(\boldsymbol{u}_{s,h}^{n+1}) \right) \, d\boldsymbol{x} \\ &+ \sum_{e \in \mathcal{E}_h^I} \frac{\varsigma_1}{2h_e} \langle [\boldsymbol{u}_{s,h}^{n+1}], [\boldsymbol{u}_{s,h}^{n+1}] \rangle_e - \sum_{e \in \mathcal{E}_h^I} \langle \{\sigma_e(\boldsymbol{u}_{s,h}^{n+1}) \boldsymbol{n}_e\}, [\boldsymbol{u}_{s,h}^{n+1}] \rangle_e. \end{aligned} \tag{23}$$

4 Numerical Examples

We design numerical experiments to validate the proposed computational framework for modeling compressible gas flow in poroelastic media. The test cases are specifically constructed to evaluate: the model's capability in capturing coupled hydro-mechanical processes, the algorithm's performance in handling strong nonlinearities and the numerical scheme's conservation properties. The simulations consider methane gas with physical properties listed in Table 1, maintaining a constant temperature of 330 K throughout all test cases.

Table 1. Physical properties of methane.

P_c(bar)	T_c(K)	Acentric factor	M_w(g/mole)	Viscosity (Pa $\cdot$ s)
45.99	190.56	0.011	16.04	10^{-5}

4.1 Example 1

In this example, we investigate the gas flow dynamics within a closed domain to rigorously validate both the physical model's accuracy and the first numerical scheme's performance in simulating compressible gas flow. The simulation serves to verify three fundamental physical principles: strict mass conservation, thermodynamic consistency in energy dissipation, and boundedness of molar density. The domain is initialized with a high-concentration zone (300 mol/m^3 molar density) at the center, surrounded by a low-concentration region (10 mol/m^3). A distinctive cross-shaped high-permeability zone ($\kappa = 100$ md) is embedded within the central area, while the remaining domain maintains low permeability ($\kappa = 1$ md). This configuration, as illustrated in Figure 1.

ICCS Camera Ready Version 2025
To cite this paper please use the final published version:
DOI: 10.1007/978-3-031-97632-2_15

Figure 2 provides critical validation of the proposed numerical scheme's ability to preserve fundamental physical properties, demonstrating strict adherence to energy dissipation principles, exact mass conservation, and molar density boundedness. Figure 3 presents the temporal evolution of molar density distribution, demonstrating the dynamic mass transport characteristics. The corresponding thermodynamic driving forces are visualized in Figure 4 through chemical potential contours, which reveal the non-equilibrium processes governing molecular diffusion.

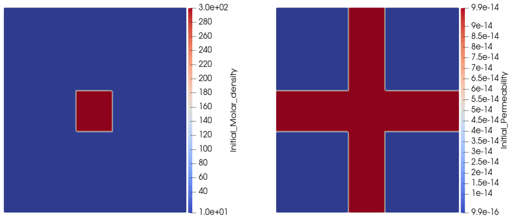

Fig. 1. Example 1: Distributions of initial molar density and permeability. Left: initial molar density. Right: initial permeability.

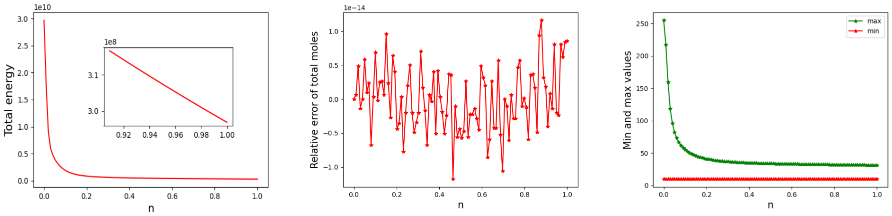

Fig. 2. Example 1: Left: System energy at different time steps. Middle: Mass conservation at different time steps. Right: Minimum and maximum values of molar density.

4.2 Example 2

To validate the performance of our second numerical scheme, we conduct the following test. We use the Perlin noise method to generate random permeability in order to simulate realistic geological scenarios, The initial molar density is obtained using $c^0 = c_0 + \text{rand}(\boldsymbol{x}) \cdot (c_1 - c_0)\,,$ where $\text{rand}(\boldsymbol{x})$ is a function for generating random numbers within the range [0,1], $c_0 = 100$ mol$/m^3$, $c_1 = 300$ mol$/m^3$. In this test, we choose $N = 10^{15}$ Pa, $\gamma = 10^{15}$ Pa , $\eta = 10^{11}$ Pa, $\delta = 0.5$. Figure 5 shows the initial molar density and permeability distribution. Figure 6 demonstrates the proposed scheme's ability to maintain energy dissipation, mass conservation, and molar density bounds. The left picture shows the energy evolution, the right two picture verify strict molar density preservation within physical bounds and mass conservation. Figure 7 illustrates the adaptive

ICCS Camera Ready Version 2025
To cite this paper please use the final published version:
DOI: 10.1007/978-3-031-97632-2_15

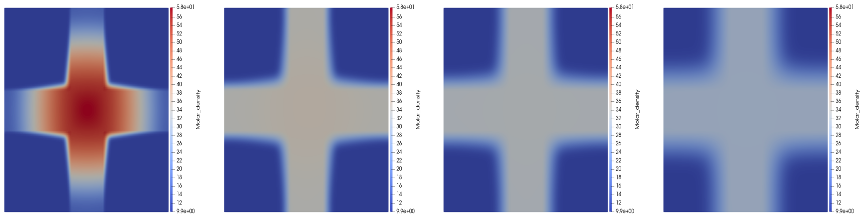

Fig. 3. Distributions of molar density at different times in Example 1. From left to right: The first: t = 0.1 h. The second: t = 0.4 h. The third: t = 0.8 h. The fourth: t = 2 h.

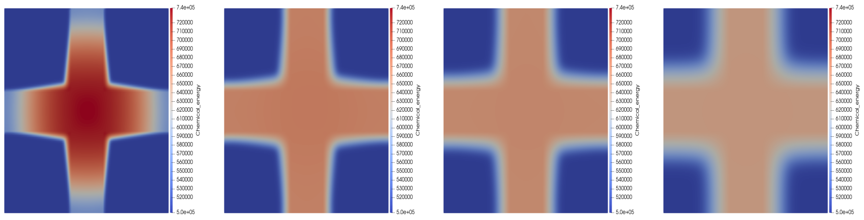

Fig. 4. Distributions of chemical potential at different times in Example 1. From left to right: The first: t = 0.1 h. The second: t = 0.4 h. The third: t = 0.8 h. The fourth: t = 2 h.

parameters: the left picture displays the dynamic stabilization parameter adjustment, while the right picture shows the time step size continuously increases as the system approaches equilibrium until reaching the preset maximum time step size $\tau_{max} = 1000$, demonstrating computational efficiency. Figure 8, Figure 9 illustrate the temporal evolution of molar density, chemical potential energy, respectively.

5 Conclusions

This paper focuses on the numerical simulation of single-phase gas flow with compressible gas and rock in the context of underground storage of hydrogen and carbon dioxide geological sequestration. It first formulates a fully coupled thermodynamic mathematical model considering the compressibility of gas and rock. Then, two energy-stable numerical schemes are proposed. The first scheme is based on an energy factorization approach, which combines a semi-implicit time-stepping formulation with a spatial discretization using discontinuous Galerkin approximations and mixed finite elements, ensuring energy dissipation and mass conservation. The second scheme, based on a stabilization approach, conserves the original energy functional, has an adaptive temporal discretization framework, and can dynamically adjust the stabilization parameter. Both schemes are proven to satisfy the energy dissipation law. Through numerical examples, including simulations in a closed domain with specific initial conditions and in a domain with randomly generated permeability, the proposed computational framework is validated. The examples demonstrate the model's ability to capture coupled hydro-mechanical processes, the algorithm's performance in handling strong nonlinearities, and the numerical scheme's conservation properties such as mass conservation and bounded molar density. This study provides a consistent and stable modeling and simulation framework with theoretical support for the engineering practice of carbon dioxide sequestration and underground storage of hydrogen.

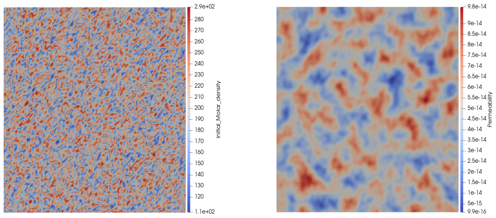

Fig. 5. Example 2: Distributions of initial molar density and permeability. Left: initial molar density. Right: initial permeability.

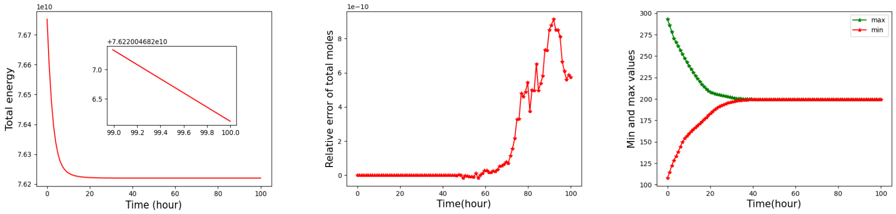

Fig. 6. Example 2: Left: Distributions of energy at different time steps. Middle: Mass conservation at different time steps. Right: Minimum and maximum values of molar density.

References

1. Chen W., Wang C., Wang X., Wise S.M.: Positivity-preserving, energy stable numerical schemes for the Cahn-Hilliard equation with logarithmic potential. J. Comput. Phys. 3, 100031 (2019).
2. Cheng Q., Shen J.: A new Lagrange multiplier approach for constructing structure preserving schemes, I. Positivity preserving. Comput. Methods Appl. Mech. Eng. 391 (6), 114585 (2022).
3. Chen H., Chen, Y., Kou J., Sun S.: An Energy-Stable Adaptive Time-Stepping Method for Modeling Compressible Gas Flow in Poroelastic Media. Preprint, 2025.

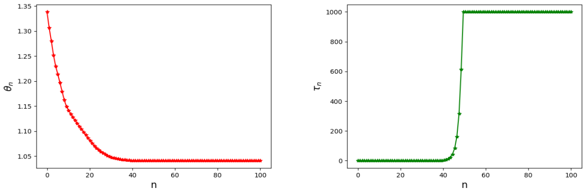

Fig. 7. Example 2: Left: Adaptive values of the stabilization parameter at different time steps. Right: Adaptive values of the time step size.

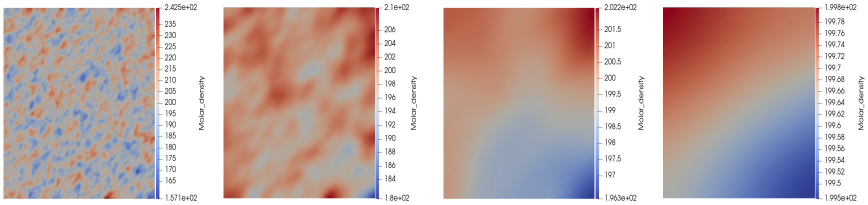

Fig. 8. Distributions of molar density at different times in Example 2. From left to right: The first: n = 10. The second: n = 30. The third: n = 30. The fourth: n = 40.

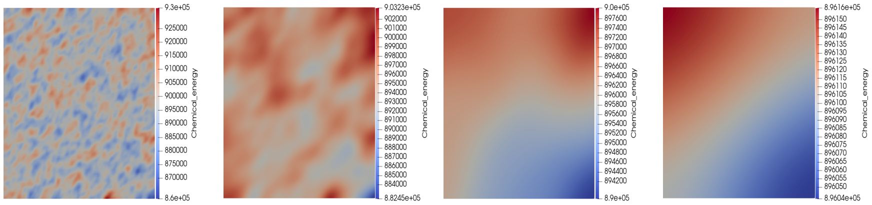

Fig. 9. Distributions of chemical potential at different times in Example 2. From left to right: The first: n = 10. The second: n = 30. The third: n = 30. The fourth: n = 40.

ICCS Camera Ready Version 2025
To cite this paper please use the final published version:
DOI: 10.1007/978-3-031-97632-2_15

4. Chen H., Chen Y., Kou J.: Energy stable finite element approximations of gas flow in poroelastic media. Comput. Methods Appl. Mech. Engrg. 428, 117082 (2024).
5. Chen Z., Huan G., and Ma Y.: Computational Methods for Multiphase Flows in Porous Media. SIAM, Philadelphia, 2006.
6. Dong L., Wang C., Wise S.M., Zhang Z.: A positivity-preserving, energy stable scheme for a ternary Cahn-Hilliard system with the singular interfacial parameters. J. Comput. Phys. 442, 110451 (2021).
7. Du Q., Ju L, Li X., Qiao Z.: Maximum bound principles for a class of semilinear parabolic equations and exponential time-differencing schemes. SIAM Review 63 , 317359 (2021).
8. Joshi V., Jaiman R.K.: A positivity preserving and conservative variational scheme for phase-field modeling of two-phase flows. J. Comput. Phys. 360, 137166 (2018).
9. Eyre D. J.: Unconditionally gradient stable time marching the Cahn-Hilliard equation, in Computational and Mathematical Models of Microstructural Evolution (San Francisco, CA, 1998). Mater. Res. Soc. Sympos. Proc. 529, MRS, Warrendale, PA, 3946 (1998).
10. Firoozabadi A.: Thermodynamics of Hydrocarbon Reservoirs. McGraw-Hill, New York, (1999).
11. Kou J., Sun S.: Thermodynamically consistent modeling and simulation of multi-component two-phase flow with partial miscibility. Comput. Methods Appl. Mech. Engrg. 331, 623649 (2018).
12. Kou J., Sun S., Wang X.: A novel energy factorization approach for the diffuse-interface model with Peng-Robinson equation of state. SIAM J. Sci. Comput. 42, B30B56 (2020).
13. Kou J., Wang X. H., Du S. G.: Energy stable and mass conservative numerical method for gas flow in porous media with rock compressibility. SIAM J. Sci. Comput., 44, B938B963 (2022).
14. Kou J., Wang X. H., Chen H. X., Sun S.: An efficient bound-preserving and energy stable algorithm for compressible gas flow in porous media. J. Comput. Phys. 473, 111751 (2023).
15. Niessner J., Helmig R.: Multi-scale modelling of two-phasetwo-component processes in heterogeneous porous media. Numer. Linear Algebra Appl. 13(9), 699715 (2006).
16. Phillips P.J., Wheeler M.: A coupling of mixed and discontinuous Galerkin finite-element methods for poroelasticity. Comput. Geosci. 12, 417435 (2008).
17. Qi R., LaForce T. C., Blunt M. J.: A three-phase four-component streamline-based simulator to study carbon dioxide storage. Comput. Geosci. 13(4), 493509 (2009).
18. Shen J., Xu J., Yang J.: The scalar auxiliary variable (SAV) approach for gradient flows. J. Comput. Phys. 353, 407416 (2018).
19. Xu C., Tang T.: Stability analysis of large time-stepping methods for epitaxial growth models. SIAM J. Numer. Anal. 44, 17591779 (2006).
20. Yang J., Yuan Z, Zhou Z.: Arbitrarily high-order maximum bound preserving schemes with cut-off postprocessing for Allen-Cahn equations. J. Sci. Comput. 90, 76 (2022).
21. Yang X., Ju L.: Efficient linear schemes with unconditionally energy stability for the phase field elastic bending energy model. Comput. Methods Appl. Mech. Eng. 315, 691712 (2017).
22. Zhang X., Shu C.-W.: On positivity-preserving high order discontinuous Galerkin schemes for compressible Euler equations on rectangular meshes. J. Comput. Phys. 229 (23), 89188934 (2010).

ICCS Camera Ready Version 2025
To cite this paper please use the final published version:
DOI: 10.1007/978-3-031-97632-2_15